Renewable Energy 253 (2025) 123552

Contents lists available at ScienceDirect

Renewable Energy

journal homepage: www.elsevier.com/locate/renene

The energy quay wall: Results from a full-scale field test

Philip J. Vardon [a,*], Marco Gerola [b], Vincent Leclercq [c], Korneel de Jong [c], Jacco Haasnoot [c], Richard Janssen [d], Patrick Stoelhorst [d], Ivaylo Pantev [c], Jorrit de Vries [c], Silvia Bersan [e], David Smeulders [f], Francesco Cecinato [b]

[a] *Department of Geoscience and Engineering, Delft University of Technology, Delft, the Netherlands*
[b] *Dipartimento di Scienze Della Terra "A. Desio", Università Degli Studi di Milano, Milan, Italy*
[c] *CRUX Engineering BV, Delft, the Netherlands*
[d] *Gooimeer BV, Almere, the Netherlands*
[e] *Hoogheemraadschap de Stichtse Rijnlanden, Houten, the Netherlands*
[f] *Department of Mechanical Engineering, Eindhoven University of Technology, Eindhoven, the Netherlands*

A R T I C L E I N F O

Keywords:
Shallow geothermal
Energy geo-structure
Field test
Thermal energy
Energy storage

A B S T R A C T

Energy Quay Walls (EQWs) are innovative energy geostructures which exchange thermal energy with both soil and open water while providing a structural function. A full-scale EQW with thermally activated sheet piles was tested, measuring 8.4 m in length along a 1.75m deep canal, with the sheet piles embedded 13m into the underlying soil. Two different length heat exchangers were used: shallow (3 m length) loops primarily extracting thermal energy from the open water, and deep (15 m length) loops extracting energy also from the soil. The shallow loops demonstrated a high heat extraction rate per activated surface area (~200 W/m^2 at 8 °C water temperature, compared with ~60 W/m^2 for the deep loops), with their performance closely linked to the open water temperature. The shallow loops did not require time to restore surrounding temperatures, indicating stable long-term performance, yet can extract the least energy at the coldest time periods. In contrast, the deeper loops exhibit greater stability across varying open water temperatures and achieve the highest total energy extraction per quay wall length (~900 W/m at 8 °C water temperature, compared with ~600 W/m for the shallow loops). Realistic operation of the deep loops lowered the soil temperature by ~2 °C.

1. Introduction

In response to the escalating global energy demand and the required reduction in carbon emissions, innovative solutions are imperative. Energy Geostructures (EGs), particularly energy piles, are an important innovation, facilitating the extraction of thermal energy from the environment, suitable for space heating and cooling. By integrating heat transfer pipes into foundations and buried geotechnical structures, EGs eliminate the necessity for dedicated ground heat exchangers, thereby presenting opportunities to mitigate capital costs associated with shallow geothermal energy systems e.g. Refs. [1–5]. Energy provision is typically the secondary purpose of the EG, with the structural performance taking priority in the design. Additionally to thermal energy extraction, EGs can function as thermal energy storage systems, e.g. during periods such as the summer months thermal energy can be stored for future use in the winter months [6,7].

To enhance the thermal and thermo-mechanical understanding of different types of EGs under real-world conditions, numerous full-scale tests have been installed globally, accompanied by comprehensive monitoring systems [8]. In the case of energy piles, well-monitored full-scale tests have been conducted in various locations, including Switzerland [9], England [10], Denmark [11], China [12], Australia [13], USA [14] and the Netherlands [15]. Energy walls have been studied in full-scale installations in England [16], Italy [17,18] and China [19]. Similarly, full-scale energy tunnel installations have been completed in Austria [20], South Korea [21,22], Germany [23] and Italy [24].

Driven by the successful outcomes of installations worldwide, recent years have seen the emergence of new EG types as innovative solutions for harnessing shallow geothermal energy. These novel structures

This article is part of a special issue entitled: Geothermal heating-cooling published in Renewable Energy.

* Corresponding author.
E-mail address: p.j.vardon@tudelft.nl (P.J. Vardon).

https://doi.org/10.1016/j.renene.2025.123552
Received 18 December 2024; Received in revised form 23 April 2025; Accepted 22 May 2025
Available online 23 May 2025
0960-1481/

include energy micropiles [25–27], climate roads [28,29], energy anchors [30], geothermal pavements [31,32], energy sewers [33], cutter soil mix energy walls [34], energy piles with phase change material [35] and energy barrettes [36].

Among these new EG types, one of the most recently proposed and novel forms of EG are so-called energy sheet piles (ESP), consisting of the integration of conventional steel sheet piles including closed-loop heat exchangers [37–39]. Energy sheet piles are part of a broader type of EG called energy walls where heat exchange occurs on a plane surface. Various experimental and modelling studies have reported a range of heat flux per activated area for energy walls typically between 10 and 50 W/m^2 [8,40], 5–30 W/m^2 [17], 12–30 W/m^2 [18], 20–40 W/m^2 [41] and 15–25 W/m^2 [42]. In all of these studies, the wall had soil on one side and air on the other. Baralis and Barla [17] presented a system where heat exchanger pipes were retrofitted to the soil side of a new or existing walls, whereas the other systems embedded heat exchanger pipes in the concrete of the wall. It was observed by Sterpi et al. [18] that the portion of the wall embedded into soil, i.e. having soil on both sides, had over double the heat flux than the portion wall with air on one side.

Energy walls have been made from piles in other situations, such as bored piles [43] (which were termed energy sheet piles, but were not made of steel sheet piles). In that work, bored piles, spaced throughout a longer wall were tested, and it was shown that both the (air) exposed and soil embedded initial and boundary conditions strongly influenced the energy performance.

Traditionally, rows of aligned sheet piles are used to form continuous watertight barriers and/or to support temporary or permanent excavations, especially for river/canal bank support along quays, where they are termed quay walls, and energy quay walls (EQWs) when they are formed from ESPs. ESPs are usually embedded in the deeper subsurface, often several times deeper than the excavation/water way they support, and therefore they are able to extract/exchange thermal energy from both the ground and surface water as thermal reservoirs.

Energy Quay Walls are considered to be applicable to provide thermal energy for both retrofitting and new-build buildings. They offer the same broad advantage of other energy geostructures that they can allow the installation of heat exchangers embedded into structural elements, eliminating the need for a separate installation. So, any building that is constructed alongside a canal could be considered. However, for retrofitting existing buildings, the structures are already built, and therefore if a quay wall is constructed, renovated or replaced adjacent to the building a cost effective ground heat exchanger can be installed. In the Netherlands, for example, many hundreds of kilometres of existing quay walls need to be renovated or replaced [44], which provides a large opportunity.

Ziegler et al. [37] first tested ESPs by carrying out large-scale laboratory tests, finding that they have a significant energy potential for renewable energy extraction from a soil/water system, and that the presence of an open water stream can greatly increase the mean thermal energy extraction rate and mean temperature difference within the loops. The highest extraction rates achieved were up to 285 W/m (length here refers to a U-tube length) without an open water stream and up to 430 W/m with an open water stream. This differs from typical ground coupled closed-loop heat exchangers or energy piles where rates after an initial peak are observed to be around 30–50 W/m [e.g. Refs. [2,45]. The open water stream was seen to result in increases of both mean thermal energy extraction rate and mean temperature difference between inlet and outlet of a maximum of around 70 %. These results demonstrated the potential of EQWs as a high performance and efficient renewable energy source, but did not delineate the impact of the soil and the open water, nor quantified the performance under field conditions.

To test the performance of EQWs created from energy sheet piles at full-scale, and in real world conditions, a bespoke full-scale test was designed and set up for the first time in De Zweth, near Delft (NL), along a canal with 1.75 m water depth, and tested from October 2020 to July 2022. The EQW system comprised 12 Z-profile sheet piles and featured three heat exchanger types characterized by steel U-loops with a rectangular cross-section, namely: *Shallow loops* and *Deep loops*, attached to the sheet piles on the soil side, respectively extending to a depth of 3 and 15 m, and 'Add-on panels,' attached the sheet piles on the water side with a depth of 3 m. The test EQW was geothermally operated with the use of a heat pump with a bespoke hydraulic and electronic control system. An extensive monitoring system was also installed to continuously measure the temperature changes in the soil, water and heat exchanger fluid, as well as fluid flowrates. The performance of heat extraction for various U-loop configurations, as well as the efficiency of underground heat storage collected from open water via the deep loops, was evaluated. Thermally-induced horizontal displacements of the EQW during geothermal operation were measured with inclinometers and determined to be negligible [46].

This paper focuses on novel insights into the performance of EQWs, focusing on the thermal behaviour of the water-ground-heat-exchanger system, and in particular the performance under different external temperatures. The quantification of heat extraction from the open water and soil under different conditions provides an important step towards system design. Initially a comprehensive description of the site and design of the test in presented, followed by an outline of the test methodology. The results and discussion focus on the performance of various heat exchanger configurations within the system, concluding with insights drawn from the test outcomes.

2. Full scale test description

In 2019, a temporary quay wall was installed in Delft (NL) to stabilize a canal bank. The canal is approximately 1.75 m deep and 35 m wide at this location, and does not have a substantial flow. The sheet piles, designed based on geotechnical considerations, extends to a depth of 16 m and has a width of 8.4 m, with various details shown in Figs. 1–4. It is composed of 12 Z-profile type ZZ17-700 sheets, each with a width of 0.7 m and a height of 0.42 m.

Prior to the quay wall installation, two cone penetration tests were conducted at the canal bottom and near the sheet pile wall to accurately identify the soil layers that are shown in Fig. 1. On the canal-facing side, the sheet pile has a length of 0.55 m in contact with the air (at the top of the piles), followed by 1.75 m in contact with the canal water, and the remainder in contact with layers of silt, silty/sandy clay, and peat. In contrast, the soil on the opposite side features a 1.85 m top layer of sand, with clay and peat extending through the entire depth of the sheet pile.

To thermally activate the quay wall, two types of steel heat exchanger loops are employed. The first type consists of incorporated loops welded directly to the quay wall's sheet pile zeta profiles, as depicted in Fig. 2a. These loops are installed up to two different depths: 3 m, referred to as *Shallow loops*, designed primarily to exchange heat with the open water, and 15 m, referred to as *Deep loops*, designed to exchange heat with both soil and open water, as shown in Fig. 1. The second type comprises steel heat exchanger pipes welded onto panels, known as *Add-on panels*, that are mounted on the quay wall, as shown in Fig. 2b. These panels also have a vertical length of 3 m and primarily exchange heat with the canal water. All the steel pipes have a rectangular cross-sectional area with outer dimensions of 40 × 20 mm^2 and a wall thickness of 3 mm. While the installation of both the Shallow loops and the Deep loops must be completed at the same time as the sheet pile installation, the Add-on panels can be mounted on pre-existing quay walls, enabling the energy retrofitting of existing sheet pile walls.

To minimize the risk of pipe damage during installation of the ESP, the U-loop's bottom part is reinforced with a steel cover, as shown in Fig. 2. Additionally, to reduce the chance of damage to the loops of the Add-on panels throughout the system's lifespan, a metal mesh is attached to the external side of the pipes (shown in Fig. 2), providing protection against any external impact and to minimize the risk of damage to both shallow and deep loops, the steel heat exchanger pipes are positioned on the soil-facing side.

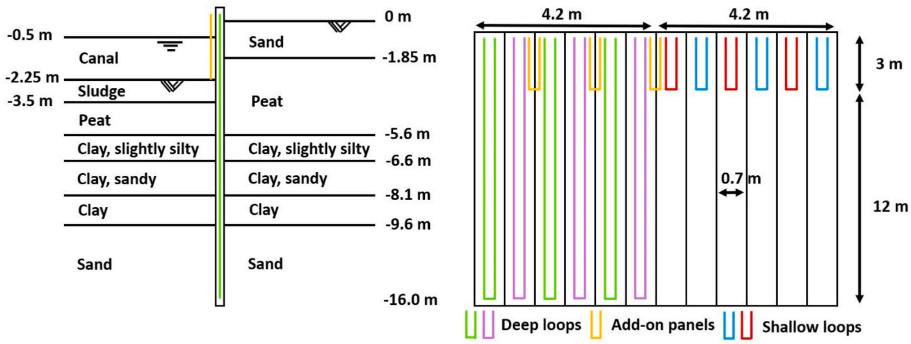

Fig. 1. Energy quay wall full scale test: soil layers and heat exchanger pipes layout.

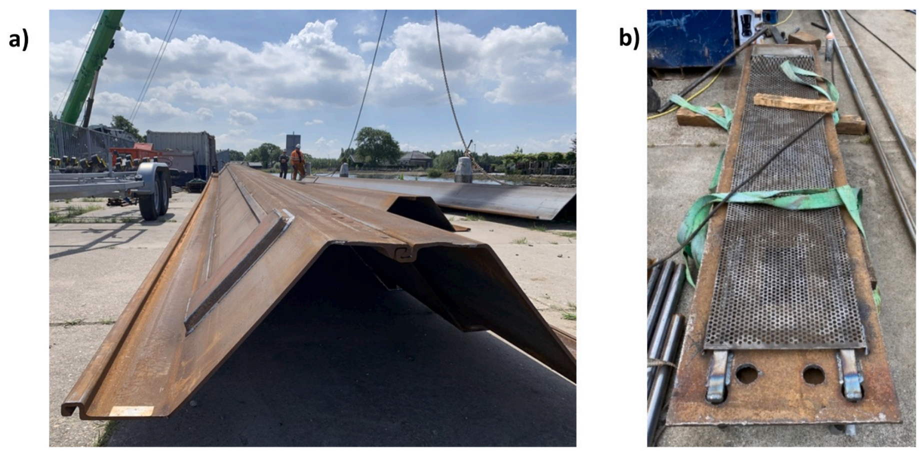

Fig. 2. Steel heat exchanger pipes welded onto the Z-profile sheet piles for a) integrated loops and b) onto panels for the Add-on configurations (right).

The hydraulic system consists of five parallel subloops, each containing three steel U-loops arranged in series, as illustrated in Figs. 1 and 3. To enable the investigation of the main objective of the paper, i.e. to investigate the performance of EQWs, focusing on the thermal behaviour of the water-ground-heat-exchanger system, each loop was designed so that it could be operated independently or together. On the left side of the EQW, two deep loop circuits (indicated schematically in green and purple on Fig. 3 and one circuit for the add-on panels (indicated in orange on Fig. 3 are installed. The right side of the EQW features two shallow loop circuits (indicated in red and blue on Fig. 3.

The steel U-loops are connected to each other and to the heat pump via high-density polyethylene (HDPE) connection pipes (see Fig. 3c), which have a diameter of 32 mm and a thickness of 2 mm. To protect the connection pipes from potential damage after the EQW installations, they are covered with a 20 cm thick sand layer. A water-glycol mixture (80 % water and 20 % monopropylene glycol) is used as the heat exchanger fluid to lower the freezing point, thereby allowing the system to operate at temperatures lower than 0 °C. During the EQW operation, the valves in the manifold, which collects all subloops, are configured to ensure equal flow velocity across each circuit. Fig. 4 shows a picture taken of both the left and right side of the EQW after its installation (prior to covering the connection pipes with sand). The heat pump system (Nibe F1155-6, 6 kW thermal) was designed to maintain a constant temperature input to the EQW and a steady flow rate within the heat exchanger pipes, to enable analysis of the EQW performance. This resulted in a variable output power due to variable heat transfer in the soil/water. To allow flexibility in testing and better investigation into the EQW performance, the heat pump was not directly connected to a building. Instead, the heat generated during the EQW full-scale test is dissipated to the air through a fan linked to the heat pump's secondary circuit, as shown in Fig. 3c.

To monitor the key parameters to assess the energy performance of the EQW full-scale tests and influence of the ground and water temperatures, various sensors were installed as shown in Figs. 3 and 4. A total of 20 thermowells (PT100, with 20 mm long sensor) were positioned within the heat exchanger pipes to monitor the temperature at both the entrance and exit of each U-loop. Flow rates across the various subloops are monitored using three digital flow meters, with a flow meter installed at the inlet of the purple deep subloop, blue shallow subloop. An additional thermowell and flowmeter were installed in the main pipe from the heat pump, along with an additional thermowell in the main pipe returning to the heat pump, enabling monitoring of the inlet and outlet temperatures as well as the overall flow rate. The canal water temperature was monitored by two sensors positioned along a single string within the canal, approximately 0.5 m from the sheet piles, with a separation of 1 m between the sensors. The flow in the canal was monitored, which indicated no prevalent and continuous flow, however the water was continuously moving at a slow rate in different directions, thought to be due to wind, boat movement and thermally-driven convection; these results are not presented further. Temperature profiles in the water and subsurface adjacent to the sheet piling was monitored using 8 thermistor strings (Geokon 3810) placed in steel pipes filled with water, with the locations shown in Fig. 3a. It is considered that the thermal energy extraction will have only a very limited impact on the canal temperature except for very locally to the heat exchanger. This is due to the large volume of water (and therefore thermal energy content) and large heat exchange area with the atmosphere, both due to the high width to depth ratio. On the deep loop activation side of the EQW, four thermistor sensor strings were installed extending to a depth of 15 m: D_C (denoting the Deep side of the test and in the Canal) and D_B (denoting the Deep side of the test and furthest Back from the canal) were positioned at 1.5 m from the EQW system, in the canal and soil,

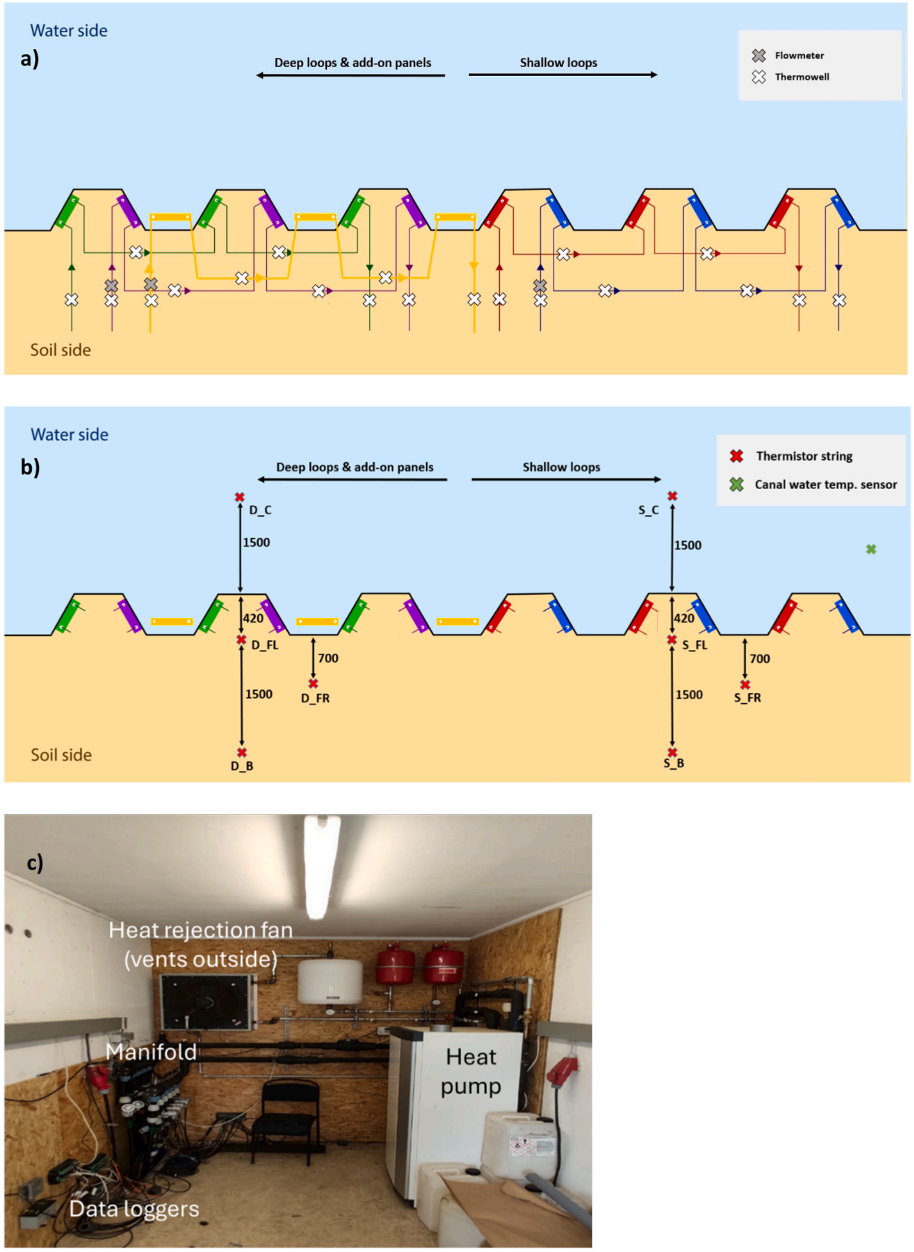

Fig. 3. Hydraulic system configuration of the EQW full-scale test, indicating the positions of a) the flowmeter and thermowell sensors, b) Thermistor string locations and c) the technical installation. The thermal activation locations are indicated with the colours corresponding to those in Fig. 1, ie green and purple are Deep loops, red and blue are Shallow loops and yellow are the Add-on panels. (For interpretation of the references to colour in this figure legend, the reader is referred to the Web version of this article.)

respectively, with sensors at 2-m depth intervals. Additionally, the sensor strings D_FL (denoting Deep Front Left) and D_FR (denoting Deep Front Right) were located at distances of 0.42 m and 0.5 m from the EQW system, respectively, with sensors at 1-m depth intervals. On the shallow loops side, four sensor strings (S_C, S_B, S_FL, and S_FR, with the S denoting the shallow side) were installed at the same distances from the EQW system as on the deep loops side, extending to a depth of 4 m. S_C string was positioned in the canal, while S_B, S_FL, and S_FR were placed in the soil. The subsurface temperature is measured at intervals of 1 m for D_FL, D_FR, S_FL, and S_FR sensors and of 2 m for D_C, D_B, S_C and S_B sensors. All sensors were connected to a datalogger (Campbell Scientific CR6 and AM16/32B multiplexer), enabling continuous data collection every 15 min.

During the test operation, some thermistor sensors failed and are not considered in this paper. Additionally, due to installation issues, temperature measurements from thermowells within the heat exchanger pipes were significantly influenced by external temperatures during the first 100 days of testing. After this period, the thermowells were replaced, yielding more accurate data, although some dependency on external temperature remained. Consequently, data from the thermowells installed within the heat exchanger pipes are excluded from the analysis presented in this paper.

Electricity usage was monitored on aggregate level in using an electricity meter to the site, as neither the heat pump performance nor the entire system installation performance was the focus of the investigation.

2.1. Test methodology

Various operational test phases, detailed in Table 1, were

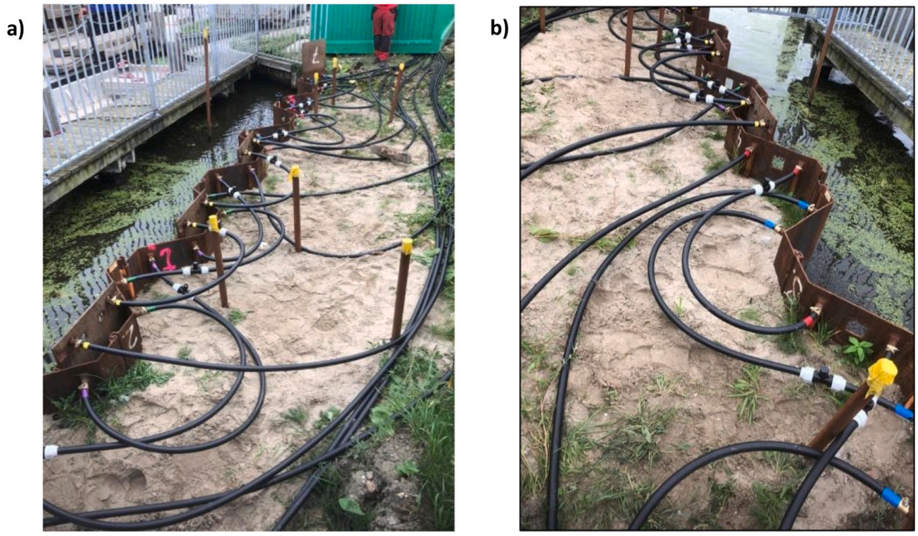

Fig. 4. Photographs of the EQW full-scale test upon completion of the installation of a) the Deep loops and Add-on panels and b) the Shallow loops.

Table 1
Overview of the EQW test phases.

Phase name	Start date	End date	Length [days]	Activated loops	Operational mode	Activated length along the canal [m]	Activated area [m^2]	Loop length [m]	Flow per group [l/s]
A	February 12, 2021	March 15, 2021	31	2 shallow loops + add-on panels	24 h a day heat extraction	7.7	23.1	54	0.13
B	March 15, 2021	March 29, 2021	14	1 shallow loop + add-on panels	24 h a day heat extraction	6.3	18.9	36	0.13
C	March 29, 2021	April 12, 2021	14	2 shallow loops	24 h a day heat extraction	4.2	12.6	36	0.13
D	April 15, 2021	June 01, 2021	47	2 deep loops	24 h a day heat extraction	4.2	63	180	0.1
E	June 01, 2021	June 30, 2021	29	None	Passive regeneration	4.2	63	180	0
F	June 30, 2021	October 01, 2021	92	2 deep loops	Active regeneration	4.2	63	180	0.1
G	December 16, 2021	January 15, 2022	30	2 deep loops	24 h a day heat extraction	4.2	63	180	0.2
H	January 15, 2022	April 01, 2022	75	2 deep loops	Intermittent heat extraction	4.2	63	180	0.2

implemented to assess the energy performance of the different subloops installed in the EQW full-scale test. The different phases aim to study the following aspects.

1. Energy performance: The goal is to evaluate the system's energy performance for different subloop combinations under a 24 h a day activation of the heat pump. The tested combinations were:
   - Phase A: Both shallow loop circuits and add-on panels. This allows an investigation of the heat exchange with open water, with the highest density of shallow loops.
   - Phase B: One shallow loop circuit (blue) and add-on panels. This allows an investigation of the heat exchange with open water, with a lower density of shallow loops as compared with Phase A.
   - Phase C: Both shallow loop circuits active. This allows an investigation of the heat exchange with open water, with the same density of shallow loops as Phase B, but allows a comparison of the Shallow loops and Add-on panels.
   - Phase D and G: Both deep loop circuits. This allows an investigation of the heat exchange with open water and soil.
2. Regeneration: natural and forced regeneration of soil temperature was tested, specifically:
   - Phase E: Both the heat pump and the circulation pump were off, allowing the soil to recover its temperature through natural conduction only.
   - Phase F: The heat pump was off while the circulation pump was on, allowing the heat exchanger fluid to transfer heat from the open water and into the soil, facilitating temperature restoration and thermal energy storage underground. Both deep loop circuits were active, as temperature had been depleted also by both loops.
3. Energy performance with real heating demand: during Phase H, the heat pump was active during two periods per day to simulate the intermittent heating demands commonly encountered in real-world applications. Both deep loop circuits were active, as the focus was on the influence on soil temperatures with lower (more realistic) average heat extraction.

3. Results and discussion

3.1. Analysis metrics

The energy efficiency of a geothermal installation can be evaluated by analysing the exchanged energy over time. The thermal power provided from the heat exchanger ($\dot{q}$) can be calculated using the following formula:

$$\dot{q} = \dot{m}\, C_p\, [T_{out} - T_{in}] \tag{1}$$

where T_{in} and T_{out} represent the inlet and outlet temperatures of the heat pump [K], respectively. $\dot{m}$ denotes the mass flow rate of the heat exchanger fluid [kg/s], and C_p represents the specific heat capacity of the heat exchanger fluid that is considered constant throughout all phases, i.e. 3690 J/kgK.

The evaluated thermal power gain is entirely attributed to the vertical steel U-loops for both shallow and deep loops. The power contribution from the HDPE pipes, which connect the sheet piling to the heat pump and link two consecutive steel U-loops, is considered negligible in comparison.

The coefficient of performance (COP) is calculated by dividing the total (thermal) energy gained by the (electrical) energy utilised for the whole system (circulation pump, heat pump and fan to exchange the produced energy with the air).

The flow type within the heat exchanger pipes is assessed using the Reynolds number (Re), calculated as follows:

$$Re = \frac{\rho v d}{\mu} \tag{2}$$

where ρ represents the density of the heat exchanger fluid which is a water 80 % -glycol 20 % mixture (1040 kg/m^3), d denotes the hydraulic diameter of the steel heat exchanger pipes (0.02 m), v [m/s] is the flow velocity within the heat exchanger pipes which depends on the selected phase, and μ corresponds to the dynamic viscosity of the heat exchanger fluid set to 2.314 mPa s.

3.2. Shallow loops

Phases A-C focus on different operational aspects of the shallow loops (see Table 1 for more details). These phases were characterized by the continuous 24 h a day operation of the heat pump, spanning a total duration of 59 days. This period occurred in early spring, during an upward trend in both external air and open water temperatures until they reached a more constant value as shown in Fig. 5. The open water temperature was seen to follow the air temperature with a small time lag, a lower magnitude of variation and without dropping below zero. During the initial 10 days of Phase A, the temperature difference between the inlet and outlet of the heat pump (as shown on Fig. 5) increased in response to rising water and air temperatures. Following this period, the temperature difference stabilized in the subsequent phases. While the inlet fluid temperature remained constant at approximately −2 °C across all phases (as shown in Fig. 5), the outlet temperature varied, reflecting changes in the open water temperature underscoring the strong correlation between the outlet temperature and the open water temperature. This strong correlation indicates that there is no temporal decline in thermal power, as is typical in ground source boreholes where heat transfer to the loops is primarily by conduction. This is attributed to heat transfer in the water being primarily by convection either by density driven flow (due to induced temperature change) or water movement due to other processes, e.g. wind. There were three intervals—two during Phase A and one in Phase C—where the inlet fluid temperature increased by few degrees over a short period. This was likely due to a heat pump malfunction.

During these phases, the flow within the pipes remained constant at 0.13 l/s. The calculated Reynolds number is 2337, which falls within the range of 2100–4000, indicating that the flow type within the heat exchanger pipes was transient but close to laminar flow.

Fig. 6 shows the temperature distribution within the first 4 m of soil recorded by the S_FL and S_FR sensors at the start of each phase and at the end of Phase C. In the upper 2 m, the soil temperature exhibited significant variation across the different phases. Despite the activation of the shallow loops and/or the addon panels, the temperature in this zone did not decrease over time but instead aligned closely with the open water temperature. For instance, at a depth of 1 m at the start of Phase A, the soil temperature was slightly above 1 °C for both S_FL and S_FR sensors, which corresponds closely to the open water temperature of 1.5 °C and was higher than the air temperature of −0.5 °C. The close alignment with the open water temperature with the soil temperature in these phases indicates that heat transfer between the soil and the water is more significant that heat transfer between the soil and the shallow loops. This is considered to imply that natural convection occurs in the open water, so that there is always thermal energy available in the water to maintain the soil temperature.

At a depth of 3 m, the temperature distribution showed less variation over time compared to the upper 2 m. This is due to the conductive heat transfer process through the soil which is slower. It is seen that between Phase A and Phase B, the soil temperature at 3 m depth is reduced due to the colder open water, and then rises in Phases B and C due to warmer open water. A cold 'bubble' is formed which first increases during Phase A and then decreases during Phases B and C. Although the temperature variation at 3 m was reduced, it still appeared to be more influenced by the open water temperature than by the heat transfer processes of the EQW system. For instance, the temperature at 3 m at the start of Phase C is higher than at the start of Phase B. This trend continues at a depth of 4 m, where the temperature differences between phases were even smaller than at 3 m. The cause of this behaviour is considered to be that heat conduction from the water to the soil is the dominant process, so below 3 m depth the temperature variation is significantly lower than in the upper section, and there is limited impact of the thermal energy extraction.

3.2.1. Heat extraction rate

The flow rate within the heat exchanger remained virtually constant

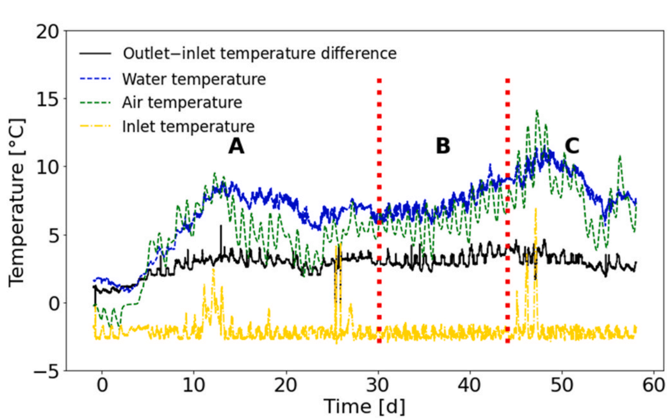

Fig. 5. Temperature difference between the outlet and inlet of the heat pump, along with water, air and inlet fluid temperatures, recorded during Phases A, B, and C.

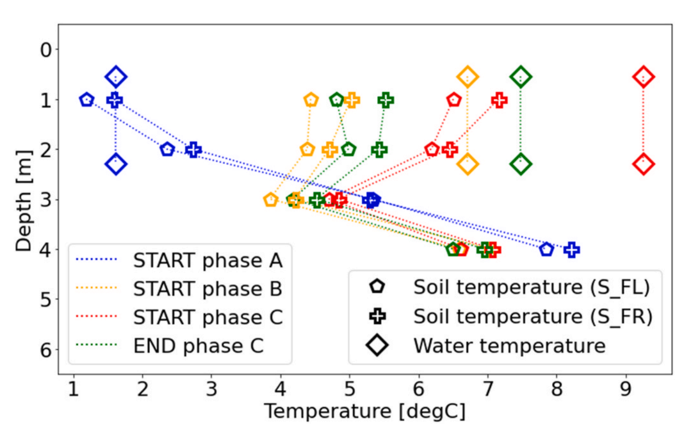

Fig. 6. Temperature profile within the soil detected from S_FL and S_FR sensors at the beginning of Phases A, B and C and at the end of Phase C alongside the open water temperature.

during Phases A, B and C. Consequently, the trend in (thermal) power gained closely mirrors the variation in temperature difference between the inlet and outlet of the heat pump. Thus, observations regarding the temperature difference variation can be extrapolated to the thermal power produced.

Fig. 7a illustrates the power gained per activated area and per activated length along the EQW as a function of the temperature difference between water and inlet fluid temperatures for the considered phases. The energy output fits a linear trend with a reasonable scatter. All the activation setups exhibit temperature differences between water and inlet temperatures ranging from 9 to 11 °C. Within this range, the configuration involving 2 shallow loops alone (Phase C) shows a moderately higher heat extraction rate per activated area compared to the combination of 1 shallow loop and add-on panels (Phase C) and the setup combining two shallow loops with add-on panels (Phase A). This disparity may be attributed to the lower density of the installation in the add on panels, increasing the activated area and length along the EQW, without increasing the loop lengths. On the other hand, the data points corresponding to Phase B exhibit a higher heat exchange rate per loop length (note that loop length is the total length of heat exchanger, which is double that of a U-tube length as often used in borehole heat exchanger calculations). This is illustrated in Fig. 7b and deviates from the linear trends observed in Phases A and C. The increased rate in Phase B can likely be attributed to the higher thermal interaction between the two shallow loops in Phases A and C, which are installed in adjacent steel quay wall profiles while the setup involving one shallow loop and

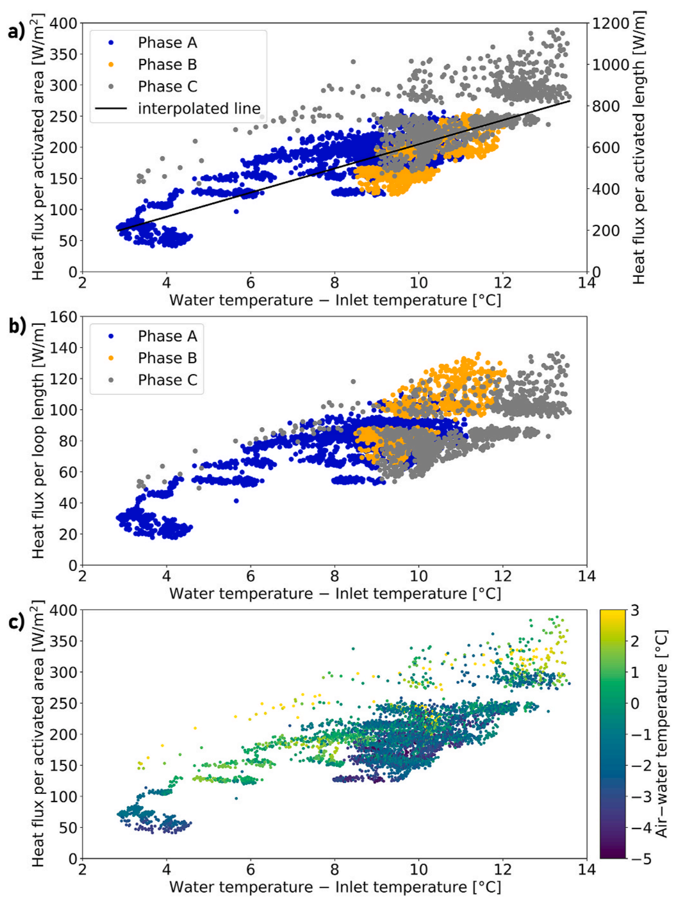

Fig. 7. Heat extraction rate of the shallow loops for Phases A, B, and C, considering every data collected from the monitoring system: a) heat flux per activated area and per activated length along the EQW plus linear interpolation b) heat flux per loop length and c) impact of air and open water temperature differences on the heat flux versus the temperature difference between open water and inlet fluid temperatures.

one add-on panel, installed on opposite sides of the quay wall, has the lowest thermal interaction between the pipes. This indicates that there is an interaction between the adjacent loops, and where feasible maximizing the activated area with a more limited number of loops can be a good design choice.

A linear interpolation can be utilised to evaluate the overall trend of the data points as shown in Fig. 7a. The resulting linear equations are:

$$q_{AREA} = (T_{WATER} - T_{INLET}) \cdot 19.4 \left[\mathrm{W/m^2K}\right] + 10.6 \left[\mathrm{W/m^2}\right] \quad (3)$$

$$q_{LENGTH} = (T_{WATER} - T_{INLET}) \cdot 58.2 \left[\mathrm{W/mK}\right] + 31.8 \left[\mathrm{W/m}\right] \quad (4)$$

where q_{AREA} is the heat flux per activated area, q_{LENGTH} is the heat flux per activated length along the canal, T_{WATER} is the open water temperature and T_{INLET} is the inlet fluid temperature. The linear interpolations both exhibit coefficients of determination (R^2) of 0.65, with root mean squared errors (RMSE) of 32.90 W/m^2 for Equation (3) and 98.70 W/m for Equation (4). These indicate that the primary relationship is captured, yet the relationship does not explain all causes. Note that this relationship will be moderately different for other densities of the loops per metre of quay wall, so it is mostly useful for initial scoping. It is important to note that the predicted heat extraction rate is evaluated for conditions where the open water remains unfrozen, with temperatures above 0 °C. The linear interpolation method may also be applicable for scenarios with frozen open water, where typically only the surface is frozen while the underlying canal water continues to flow, but data is not available to demonstrate this. When the open water temperature equals the inlet fluid temperature, the heat exchange rate is theoretically expected to approach zero; however, using the interpolated line, it yields values of 10.6 W/m^2 or 31.8 W/m for activated area or activated length, respectively, so this relationship should be used with care with low temperature differences.

The scatter in the data points is primarily due to various factors influencing the heat extraction rate that are not represented in the chart, such as air temperature, that impacts the connecting pipes between the loops and the heat pump. In Fig. 7c, the same data is presented as in Fig. 7a, coloured by the difference between the air and water temperature. Most points on the lower bound correspond to situations where air temperature was lower than the open water temperature, which negatively impacts the overall energy efficiency of the EQW system. Conversely, when air temperature exceeded open water temperature, the points tend to cluster on the upper bound of the distribution. Additional influences on the data point scatter include soil temperature (which reduces with ongoing energy extraction), annual variations in canal depth (approximately 20–30 cm), and the velocity and direction of the open water flow.

3.3. *Deep loops*

3.3.1. *Continuous operation – Phase D*

Phase D comprised the continuous operation of the heat pump over a 24-h cycle. Spanning a duration of 47 days, extending from April 15th to June 1st, 2021. This temporal interval, transitioning from spring to early summer, witnessed a predominant upward trend in both air and open water temperatures illustrated in Fig. 8. The air temperature showed higher daily temperature fluctuations, ranging between approximately 4 to 8 °C. Conversely, the open water temperature experienced fluctuations below 1 °C on most days. The water temperature is at the higher end of the range of the air temperatures throughout, thought to be mainly due to the impact of solar radiation and higher thermal mass of the water. The extractin is considered to have a negigible impact due to the extraction amount being low compared to the overall thermal energy content.

Flow within the pipes remained constant at 0.1 l/s during this phase resulting in a Reynolds number equal to 1905. With the Reynolds number falling below 2100, the flow is identified as laminar. Both the

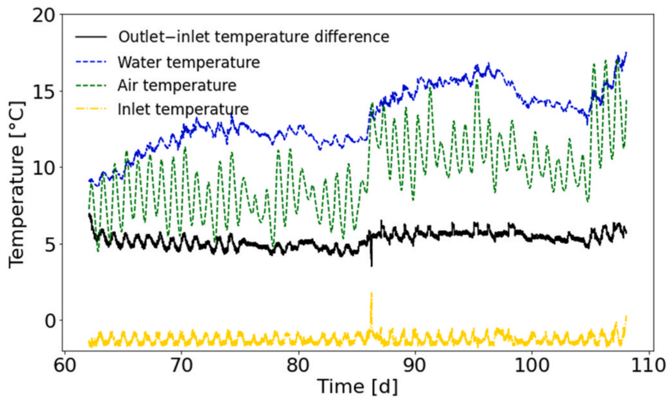

Fig. 8. Temperature difference between the outlet and inlet of the heat pump, along with water, air and inlet fluid temperatures, recorded during Phase D.

inlet fluid temperature, depicted in Fig. 8, and outlet temperature of the heat pump remained relatively constant. Daily fluctuations of approximately 0.5 °C of the outlet minus inlet fluid temperature difference can be attributed to the daily variation of water and air temperature. A marginal increase after the 195-day mark correlates with the rising temperatures of both the water and air.

On the initial day of Phase D, a high temperature difference between the inlet and outlet was observed. Subsequently, a gradual reduction in both the temperature difference and the outlet temperature persisted until day 95, with a decelerating rate, even though the open water temperature rose. This behaviour is predominantly linked to the decreasing soil temperature with ongoing energy extraction. The heat transfer towards the loops is considered to be a combination of convection in the water and conduction in the soil. The slower conduction process is responsible for the decelerating heat transfer rate.

The D_FL and D_FR thermistor strings, which have the highest number of thermistors, are utilised to analyse temperature variations within the 15-m soil profile. To improve visibility of the analysis, an averaging approach is adopted, averaging measurements from sensors located at depths of 1–5 m, 6–10 m, and 11–15 m, with the results shown in Fig. 9. It is observed that the temperature averages derived from depths of 6–10 m and 11–15 m exhibit a consistent decrease throughout the entire phase with the latter showing a smaller decrease than the former, confirming the slower heat transfer in the soil due to conduction. This discrepancy is attributed to the different thermal properties of the soil: sandy layers, present between 6 and 10 m depth, exhibit a higher thermal diffusivity, whereas clay soil at greater depths demonstrates a lower thermal diffusivity. Furthermore, the thermistors situated at the lowest depths within the string extended slightly beyond the base of the heat exchanger U-loop, leading to a reduced temperature fluctuation. The temperature trend associated with the average taken from 1 to 5 m depth is closely linked to the water and air temperature rather than influenced by the heat extraction from the energy quay wall – consistent with the behaviour seen in Phases A to C.

The temperature profiles detected from the D_FL and D_FR thermistor strings at the start and end of Phase D, shown in Fig. 10, show the impact of heat extraction on soil temperatures at depths higher than 4 m. In the initial 3 m, it is observed that the temperatures at the end were approximately equivalent or exceeded those at the start of Phase D. Notably, the D_FL thermistor string showed a higher temperature variation between the start and end of the phase compared to the D_FR sensor. This difference is attributed to the closer proximity of the D_FL thermistor string to the EQW.

3.3.2. *Long-term operation – Phase H*

Phase H encompasses the long-term operation of the system, characterized by two daily activation periods, each lasting 7-8 h—one in the morning and another in the afternoon. Phase E spanned 74 days, from January 15th to April 1st, 2021. During this temporal interval, transitioning from winter to early spring, the recorded water and air temperatures exhibited a notable decrease compared to previous phases, with a predominant upward trend observed in both air and open water temperatures, as shown in Fig. 11.

Flow within the pipes remained constant at 0.2 l/s during this phase, resulting in a Reynolds number of 3600, i.e. transient conditions close to turbulent. Fig. 11 shows the temperature difference between the outlet and inlet of the heat pump when the heat pump was operational. Each time the heat pump transitioned from off to on, the temperature difference between the outlet and inlet initiated from a high value and gradually decreased in the subsequent hours. During the off state, the heat exchanger fluid reached thermal equilibrium with the soil and water, resulting in a higher temperature at the outlet when the fluid again began circulating.

The initial temperature within the soil was observed to be lower than that recorded in Phase D. This temperature reduction occurred during Phase G, before Phase H, when the deep loops were in operation for a duration of 34 days. The soil temperature did not demonstrate a distinct recovery when the heat pump was inactive, as illustrated in Fig. 12, due to the distance between the loops and the sensors.

3.3.3. *Long-term operation vs continuous operation – Phases D, G and H*

To better understand the soil temperature decrease, a comparative analysis is conducted between Phase H for long-term heat pump operation and Phases D and G for continuous operation. This was done over the first 29 days of operation to ensure a fair comparison. The temperature differences within the soil between the end and the start are calculated for the three different depth ranges for each phase. These

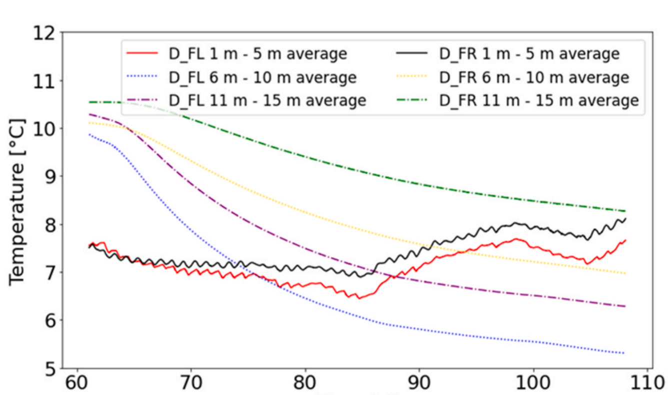

Fig. 9. Average temperature variation within the soil across depths of 1–5 m, 6–10 m, and 11–15 m for D_FL and D_FR sensors during Phase D.

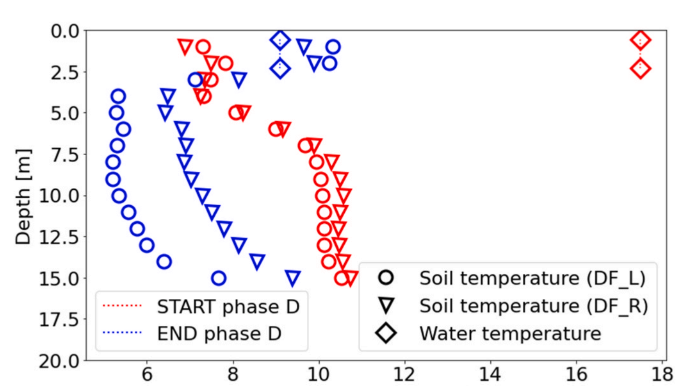

Fig. 10. Temperature profile within the soil as measured by D_FL and D_FR sensors at the start and end of Phase D alongside the open water temperature.

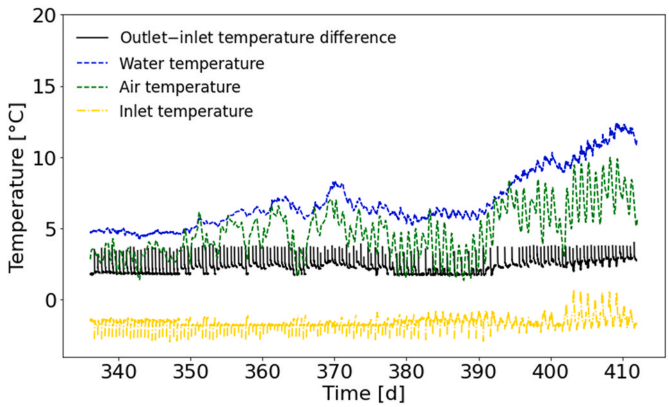

Fig. 11. Temperature difference between the outlet and inlet of the heat pump, along with inlet, water and air temperatures, recorded during Phase H. The heat pump temperature difference and the inlet fluid temperature are shown only during the heat pump operational periods.

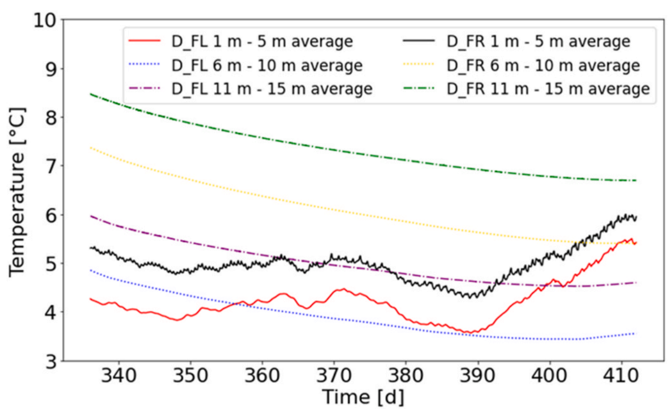

Fig. 12. Average temperature variation within the soil across depths of 1–5 m, 6–10 m, and 11–15 m for D_FL and D_FR sensors during Phase H.

values are then divided by the total number of days the heat pump was active during the phase, which is equal to the phase duration in the case of continuous operation and is lower than the phase timespan for long-term operation, as shown in Fig. 13.

For the 1–5 m depth range, the values vary significantly for each case, as the temperature in this uppermost layer of the subsurface depends on water and air temperature values. Examining the 6–10 m and 11–15 m depth ranges, the values are associated with the EQW energy extraction process. Specifically, for the D_FL thermistor string, during continuous operation phases (Phases D and G), the soil temperature decreases by up to 0.14 °C and 0.125 °C for the 6–10 m and 11–15 m depth ranges, respectively while Phase H shows only a decrease of 0.04 °C per day for both the depth ranges. Despite the heat pump being active for a total of 55 days out of the 76 days in Phase H, the impact on the soil temperatures is less pronounced compared to continuous activation.

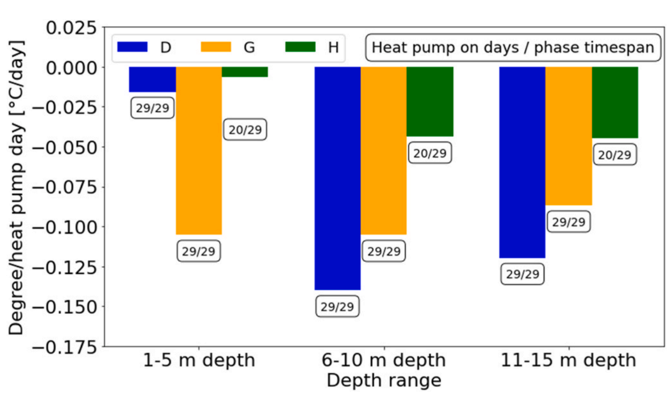

Fig. 13. Average soil temperature changes per heat pump activation day, as detected by the D_FL sensor, for depth ranges of 1–5 m, 6–10 m, and 11–15 m during Phases D, G, and H. The circled numbers at the bottom of each column indicate the total days the system was active (left number) in comparison to the total days in the phase (right number).

3.3.4. Passive vs active regeneration – Phases E and F

Phases E and F, which occurred during a period of elevated water and air temperatures, were carried out to represent periods where heat extraction was not needed, and the soil temperature could be restored. Phase E, named the passive regeneration phase, spanned 28 days from June 2nd, 2021, to June 30th, during which both the heat pump and circulation pump were inactive. In the initial 20 days, air and open water temperatures increased by approximately 10 °C, reaching 25 °C, followed by a 5 °C decrease as shown in Fig. 14. Phase F, named the active regeneration phase, extended over 93 days from June 30th to October 1st, with the heat pump inactive and the circulation pump operational, maintaining a constant flow velocity of 0.24 m/s within the heat exchanger pipes. During this period, air and open water temperatures remained relatively stable around 20 °C, with a minor decline observed in the final days.

As depicted in Fig. 15, the temperature within various depth ranges at the start of the passive regeneration phase were lower than the undisturbed temperature (12 °C). This discrepancy is due to the prior operation of the deep loops. Over the course of the passive regeneration phase, the average temperature recorded from 1 to 5 m depth experienced an increase of approximately 7 °C, primarily linked to the concurrent rise in water and air temperatures during this period. Conversely, the temperatures in deeper ranges showed an increase of 2 °C, representing heat recovery through natural conduction only, mostly in a vertical direction from the surface. In the active regeneration phase, the temperatures at the phase's start were still lower than the undisturbed temperature, except for the average recorded from 1 to 5 m depth. Temperatures across all depth ranges exhibited a continual increase throughout the entire phase with a high gradient at the start reducing in time. By the conclusion of Phase F, temperatures in different depth ranges surpassed 12 °C, indicating not only the restoration of soil temperature but also the storage of heat extracted from the open water, forming a 'heat bubble' in the soil surrounding the EWQ.

In Phase E, both the heat pump and the circulation pump were inactive, causing the heat exchanger fluid to remain stagnant. During this period, the detected inlet and outlet temperatures of the heat pump were influenced only by external temperatures and they were excluded

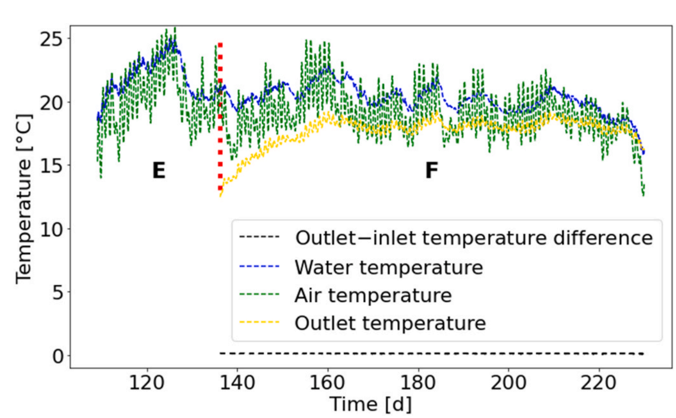

Fig. 14. Temperature difference between the outlet and inlet of the heat pump, along with inlet, water and air temperatures, recorded during Phases E and F.

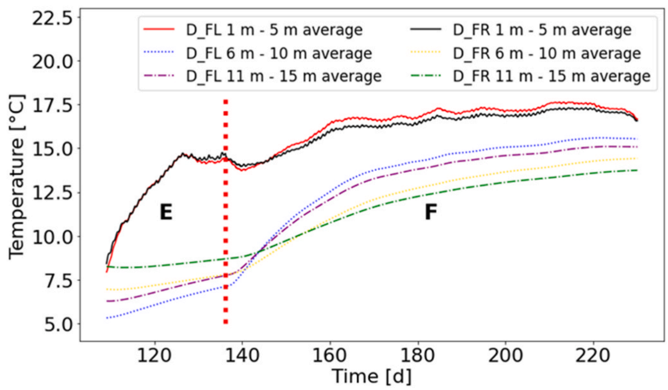

Fig. 15. Average temperature variation within the soil across depths of 1–5 m, 6–10 m, and 11–15 m for D_FL and D_FR sensors during Phases E and F.

from Fig. 14. When the active regeneration phase starts, the circulation pump was activated, initiating fluid flow within the heat exchanger pipes. In the first month of this phase, the inlet and outlet temperatures started at 12.5 °C and rose rapidly, closely following the open water temperature. For the remainder of Phase F, the inlet and outlet temperatures stabilized, and the soil temperature increased at a slower pace, again indicative of the soil thermal conduction process. When the soil temperature was below the undisturbed temperature, the active regeneration phase facilitated a quicker restoration of ground temperature compared to when the temperature was above the undisturbed level.

3.3.5. Heat extraction rate

Fig. 16a illustrates the (thermal) power gained per activated area and per activated length of the quay wall along the canal of the deep loops, as a function of the temperature difference between water and inlet fluid temperatures. The data from Phase D spanned a different and larger range of temperature difference compared to Phases G and H, making comparison challenging. The heat extraction rate points within the

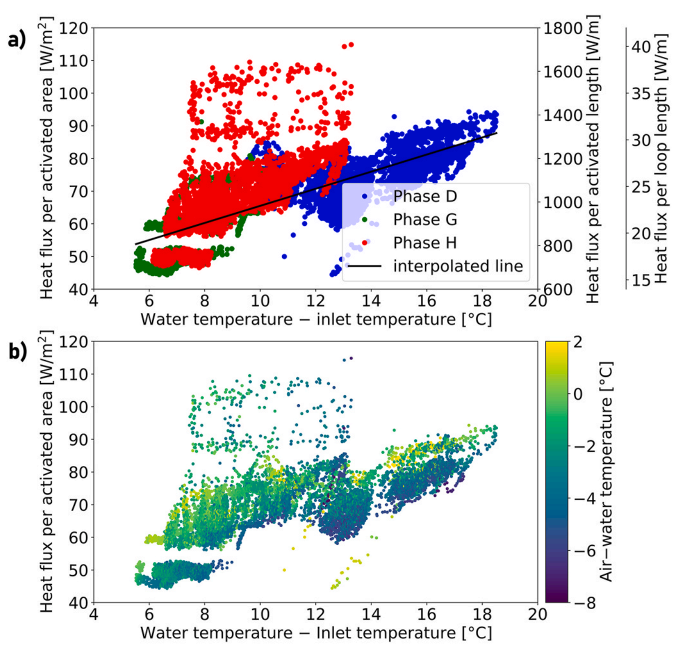

Fig. 16. Heat extraction rate of the deep loops for Phases D, G, and H, considering every data collected from the monitoring system: a) heat flux per activated area, per activated length along the EQW and per loop length plus linear interpolation b) impact of air and open water temperature differences on the heat flux versus the temperature difference between open water and inlet fluid temperatures.

9–11 °C temperature difference range in Phase D correspond to the initial 5 days of this phase. This period was characterized by the system's transient behaviour, where both the outlet temperature of the heat pump and the soil temperature decreased rapidly. Similarly, the highest points for Phase G are also related to its first 5 days. Phase H shows some points with a heat extraction rate per activated area exceeding 90 W/m^2, which are linked to the activation of the heat pump. Specifically, the first two points after the heat pump was turned on are influenced by the higher temperature of the heat exchanger liquid that was reached when the system was off. A similar analysis applies to the heat flux per unit loop length, as shown in Fig. 16a.

Similar to the approach used for the shallow loops, a linear interpolation is employed to evaluate the overall trend of the data points, as shown in Fig. 16b. Data corresponding to highly transient portions of the EQW system behaviour are excluded, i.e., the first 5 days of Phases D and G, as well as the first 30 min of each heat pump activation in Phase H. The resulting linear equations are:

$$q_{AREA} = (T_{WATER} - T_{INLET}) \cdot 3.0 \left[\mathrm{W/m^2K}\right] + 30.8 \left[\mathrm{W/m^2}\right] \tag{5}$$

$$q_{LENGTH} = (T_{WATER} - T_{INLET}) \cdot 45.0 \left[\mathrm{W/mK}\right] + 462.0 \left[\mathrm{W/m}\right] \tag{6}$$

The linear interpolations exhibit an R^2 of 0.53, with RMSE of 8.31 W/m^2 for Equation (5) and 124.65 W/m for Equation (6). The lower coefficient of determination than those relating to equations (3) and (4) are generally driven by Phase H, where the operating conditions are different (not run continuously). Similar to the shallow loops, the predicted heat extraction rate is evaluated under conditions where the open water remains unfrozen, with temperatures above 0 °C. When the open water temperature equals the inlet fluid temperature, the heat exchange rates determined using the interpolated lines are 30.8 W/m^2 per activated area and 460 W/m per activated length. In this scenario, thanks to the 12 m depth of the quay wall embedded in the soil, heat is extracted from the soil layers, enhancing the system's energy efficiency even at very low open water temperatures. This may offer an avenue in system design to provide peak power in very cold periods.

The dispersion of data points is influenced by factors similar to those affecting the shallow loop, such as air temperature, albeit with a reduced dispersion under similar operating conditions due to the fact that a portion of the total energy extracted by the deep loops comes from the soil, which is less dependent on external temperature fluctuations and the characteristics of the open water.

3.4. Comparison between shallow and deep loops

To compare the heat extraction rates of shallow and deep loops, the two interpolated lines are shown in Fig. 17, considering both the activated area and the activated length of the EQW. These lines extend to a temperature difference of 0 °C between the water and the inlet fluid temperature. The higher heat extraction rate per activated area for the shallow loops, compared to the deep loops, underscores the significant potential for heat extraction from open water. The deep loops only outperform the shallow loops when the temperature difference between the water and inlet is close to 0 °C. However, when considering heat flux per activated length of the EQW, the deep loops perform better due to the substantially greater length of heat exchanger loops and the energy extracted from the soil. As the temperature difference between the water and the inlet fluid increases, the heat flux per unit activated area of the shallow loops approaches that of the deep loops. This convergence occurs because part of the heat extracted from the open water in the deep loops is used to heat the soil, thereby lowering the overall energy efficiency of the deep loops. For the longer loops, additional capital expense is incurred for the welded metal heat exchanger loops, which must be considered against the additional energy yield. Importantly, the additional energy yield occurs during the coldest periods where heating demands are the highest.

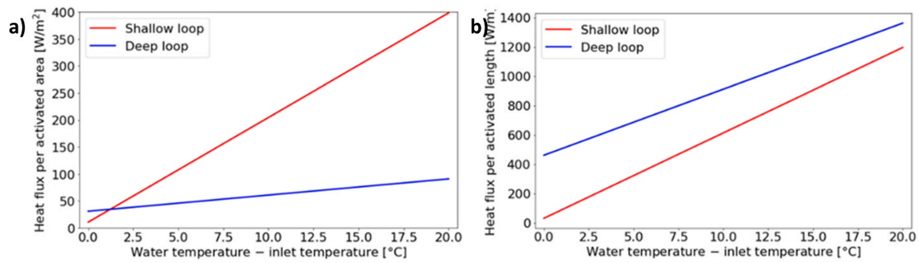

Fig. 17. Comparison of heat flux between shallow and deep loops per a) activated area and b) length of EQW.

3.5. Coefficient of performance – COP

The system was designed to test the energy yield from an EQW in different situations, and therefore the energy system (heat pump etc.) was not optimised. Nevertheless, the COP of the test system holds interesting information as a minimum value that could be achieved, which is shown in Fig. 18. The electricity usage was only recorded at a test aggregate level (including all mechanical apparatus, specifically the heat pump, circulation pumps and the dry cooler used as the heat sink) in periods of a month during the final 8 months of the test, therefore the COP is shown on a monthly basis. The period recorded was during Phase H, and a later part of the testing programme not reported here (May to July 2022).

The COP (see Fig. 18a), always referring to the heating mode, was reasonably constant around 4 in the period of December to April, when the open water temperature was also reasonably constant, rising when the open water temperature rose (May to July) (shown in Fig. 18b).

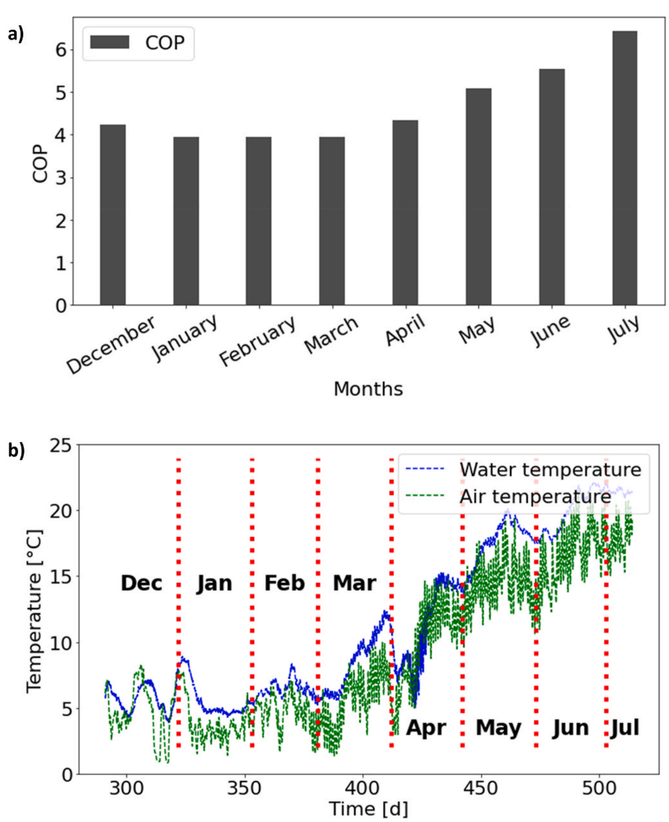

Fig. 18. a) COP values for the final 8 months of EQW operation b) Water and air temperatures recorded during the last 8 months of thermal operation of the EQW.

4. Discussion

The EQW can be installed anywhere a quay wall needs to be replaced or refurbished, and therefore offers advantages over energy geo-structures that are a part of the building which requires heating. The EQW has between about double and 5 times the heat extraction rate of energy wall systems found in the literature (depending on whether comparing with the deep or shallow loops) due to the high level of extraction possible from the open water compared to air in the literature cases. This means that the length of loops to heat (or cool) a building is much lower.

This high heat exchange rate in comparison with energy walls (between double and 5 times the rate depending on whether comparing with the deep or shallow loops), is considered to have a negligible impact on the canal temperature. However, this depends on the size and environmental conditions of the canal. In this field test, the canal is estimated to have a heat capacity around 250 MJ/K/meter of the canal, which is large considering the kW range of extraction. The wide canal is able to replenish the energy content from solar radiation and sensible heat transfer with the atmosphere. Therefore, environmental impact is considered to be minor, even with the quay wall thermally activated along the full canal length. However, in the winter, by extracting thermal energy the temperatures are reduced and there is a low amount of energy available. In the summer, this is the opposite. Therefore, there is an opportunity to combine energy quay walls with seasonal thermal storage (e.g., aquifer thermal energy storage) to take advantage of large amounts of thermal energy available in the summer, and thereby creating a positive environmental impact. This can further reduce the length of heat exchangers which would need to be installed, however would create a more complex energy system.

The heat exchange loops on the energy sheet piles that form the EQW are made from steel. This aids easy construction as they can be pushed in with the sheet pile and do not easily become damaged. In addition, the loops are installed on the soil side of the sheet pile, reducing the possibility of damage from boat (or other) collisions. However, steel is susceptible to corrosion. Steel corrosion occurs primarily when oxygen and water are in contact with the soil. In quay walls, this is observed to occur in the 'splash zone' just above the water line. Again, by placing the heat exchanger loops on the soil side of the sheet pile, splashing is removed. No corrosion was observed at the end of the test after more than two years.

5. Conclusions

The full-scale test results demonstrate that the EQW system provides a viable and efficient solution for heating applications, with the open water temperature emerging as the primary factor influencing its energy performance. The heat extraction rate of shallow loops and add-on panels exhibits a strong correlation with open water temperature. The shallow loops and add-on panels behave independently of temperature recharge, and therefore have long-term stability. These systems also display a significantly higher heat flux per activated surface area (and loop length) compared to deep loops in most scenarios (~200 W/m^2 at

8 °C water temperature, compared with ~60 W/m^2 for the deep loops).

In contrast to shallow loops and add-on panels, deep loops exhibit less sensitivity to open water temperature fluctuations, making their energy extraction more stable during colder periods, particularly when the open water temperature is low. During peak heating demand, typically in the coldest months, deep loops achieve higher thermal energy extraction per activated EQW length than the shallow loops and add-on panels. Given that the cost difference between shallow and deep loops is mainly attributed to the extended length of steel heat exchanger pipes—an inexpensive component relative to overall costs—deep loops offer a cost-effective and efficient solution for maximizing total energy extraction in EQW systems.

The system achieves its highest efficiency during the summer months, with a COP exceeding 6, although during this period, heating demand is minimal. However, the EQW system can be utilised to produce energy that can be stored. This is accomplished by activating deep loops to extract heat from the open water body and store it underground, thereby enhancing or maintaining the efficiency of deep loops by raising (restoring or elevating) soil temperatures. Coupling EQWs with shallow loops or add-on panels, which are more efficient at higher open water temperatures, enhances the potential for heat storage, particularly when integrated with other underground thermal energy storage systems.

Finally, the proposed linear interpolation between the heat flux per activated area (or length) and the temperature differential between water and inlet fluid temperature provides a quick and valuable tool for the preliminary estimation or design of EQW system energy efficiency.

CRediT authorship contribution statement

Philip J. Vardon: Writing – review & editing, Validation, Supervision, Methodology, Investigation, Formal analysis, Data curation, Conceptualization. **Marco Gerola:** Writing – original draft, Validation, Investigation, Formal analysis, Data curation. **Vincent Leclercq:** Writing – review & editing, Validation, Investigation, Formal analysis, Data curation. **Korneel de Jong:** Supervision, Resources, Project administration, Methodology, Funding acquisition, Conceptualization. **Jacco Haasnoot:** Supervision, Resources, Project administration, Methodology, Funding acquisition, Conceptualization. **Richard Janssen:** Supervision, Resources, Project administration, Funding acquisition, Conceptualization. **Patrick Stoelhorst:** Supervision, Resources, Project administration, Methodology, Funding acquisition, Conceptualization. **Ivaylo Pantev:** Validation, Investigation, Formal analysis, Data curation. **Jorrit de Vries:** Validation, Investigation, Formal analysis, Data curation. **Silvia Bersan:** Validation, Investigation, Formal analysis, Data curation. **David Smeulders:** Supervision. **Francesco Cecinato:** Writing – review & editing, Validation, Supervision, Investigation, Formal analysis, Data curation.

Declaration of competing interest

Richard Janssen and Patrick Stoelhorst have patent #EP 2 374 942 B1 and EP 3 486 378 B1 licensed to Energiedamwand (a joint venture of CRUX and Gooimeer). The other authors declare that they have no known competing financial interests or personal relationships that could have appeared to influence the work reported in this paper.

Acknowledgements

The test results, knowledge and product development are partly funded by the European-funded 'Kansen voor West' programme project 'S.P.O.E.D. KvW3-00036 and the SBIR grant from the Province of South Holland and the Netherlands Enterprise Agency. M. Gerola and F. Cecinato acknowledge support under the Italian Ministry of Universities' "PON - DM 1061/2021" scheme, co-funded by CRUX Engineering BV.

References

[1] H. Brandl, Energy foundations and other thermo-active ground structures, Géotechnique 56 (2) (2006) 81–122, https://doi.org/10.1680/geot.2006.56.2.81.
[2] F. Cecinato, F.A. Loveridge, Influences on the thermal efficiency of energy piles, Energy (Calg.) 82 (2015) 1021–1033, https://doi.org/10.1016/j.energy.2015.02.001.
[3] L. Laloui, M. Nuth, L. Vulliet, Experimental and numerical investigations of the behaviour of a heat exchanger pile, Int. J. Numer. Anal. Methods GeoMech. 30 (8) (2006) 763–781, https://doi.org/10.1002/nag.499.
[4] L. Laloui, M. Nuth, Numerical modelling of the behaviour of a heat exchanger pile, Rev. Eur. Génie Civ. 9 (5–6) (2005) 827–839, https://doi.org/10.1080/17747120.2005.9692787.
[5] F. Loveridge, F. Cecinato, Thermal performance of thermoactive continuous flight auger piles, Environmental Geotechnics 3 (4) (2016) 265–279, https://doi.org/10.1680/jenge.15.00023.
[6] F. Dupray, L. Laloui, A. Kazangba, Numerical analysis of seasonal heat storage in an energy pile foundation, Comput. Geotech. 55 (2014) 67–77, https://doi.org/10.1016/j.compgeo.2013.08.004.
[7] S.S. Meibodi, F. Loveridge, The future role of energy geostructures in fifth generation district heating and cooling networks, Energy (Calg.) 240 (2022), https://doi.org/10.1016/j.energy.2021.122481.
[8] A. Di Donna, M. Barla, T. Amis, Energy geostructures: analysis from research and systems installed around the world. DFI 2017: 42Nd Annual Conference on Deep Foundations, 2017.
[9] D. Pahud, M. Hubbuch, Measured thermal performances of the energy pile System of the dock midfield at Zürich airport. Proceedings European Geothermal Congress 2007, 2007.
[10] P.J. Bourne-Webb, B. Amatya, K. Soga, T. Amis, C. Davidson, P. Payne, Energy pile test at lambeth college, London: geotechnical and thermodynamic aspects of pile response to heat cycles, Géotechnique 59 (3) (2009) 237–248, https://doi.org/10.1680/geot.2009.59.3.237.
[11] S.E. Poulsen, M. Alberdi-Pagola, D. Cerra, A. Magrini, An experimental and numerical case study of passive building cooling with foundation pile heat exchangers in Denmark, Energies 12 (14) (2019), https://doi.org/10.3390/en12142697.
[12] G. Kong, R. Li, H. Deng, Q. Yang, Behaviours of a belled energy pile under heating-cooling cycles, J. Build. Eng. 72 (2023), https://doi.org/10.1016/j.jobe.2023.106652.
[13] M. Faizal, A. Bouazza, J.S. Mccartney, C. Haberfield, Axial and radial thermal responses of an energy pile under a six storey residential building, Can. Geotech. J. 56 (7) (2019) 1019–1033, https://doi.org/10.1139/cgj-2018-0246.
[14] C.G. Olgun, G.A. Bowers, Experimental investigation of energy pile response for bridge deck deicing applications, DFI Journal 10 (1) (2016) 41–51, https://doi.org/10.1080/19375247.2016.1166314.
[15] M. Rafai, D. Salciarini, P.J. Vardon, Full-scale in-situ tests on a displacement cast in situ energy pile: effects of cyclic thermal loads under different mechanical load levels on pile stress and strain, Geomechanics for Energy and the Environment 40 (2024) 100606, https://doi.org/10.1016/j.gete.2024.100606.
[16] T. Amis, C.A.W. Robinson, S. Wong, C. Seinuk, Integrating geothermal loops into the diaphragm walls of the Bulgari Hotel Knightsbridge London, 11th DFI/EFFC International Conference (2011). https://www.researchgate.net/publication/305699493.
[17] M. Baralis, M. Barla, Development and testing of a novel geothermal wall system, International Journal of Energy and Environmental Engineering 12 (4) (2021) 689–704, https://doi.org/10.1007/s40095-021-00407-y.
[18] D. Sterpi, G. Tomaselli, A. Angelotti, Energy performance of ground heat exchangers embedded in diaphragm walls: field observations and optimization by numerical modelling, Renew. Energy 147 (2020) 2748–2760, https://doi.org/10.1016/j.renene.2018.11.102.
[19] C. Xia, M. Sun, G. Zhang, S. Xiao, Y. Zou, Experimental study on geothermal heat exchangers buried in diaphragm walls, Energy Build. 52 (2012) 50–55, https://doi.org/10.1016/j.enbuild.2012.03.054.
[20] J.N. Franzius, N. Pralle, Turning segmental tunnels into sources of renewable energy, Proc. Inst. Civ. Eng.: Civ. Eng. 164 (1) (2011) 35–40, https://doi.org/10.1680/cien.2011.164.1.35.
[21] C. Lee, S. Park, H.J. Choi, I.M. Lee, H. Choi, Development of energy textile to use geothermal energy in tunnels, Tunn. Undergr. Space Technol. 59 (2016) 105–113, https://doi.org/10.1016/j.tust.2016.06.014.
[22] C. Lee, S. Park, J. Won, J. Jeoung, B. Sohn, H. Choi, Evaluation of thermal performance of energy textile installed in Tunnel, Renew. Energy 42 (2012) 11–22, https://doi.org/10.1016/j.renene.2011.09.031.
[23] A. Csesznák, R. Järschke, M. Wittke, B 10 Rosenstein Tunnel – designing a geothermal energy system in a spa protection area/B 10-Rosensteintunnel – planung einer Geothermieanlage im Heilquellenschutzgebiet, Geomechanik Und Tunnelbau 9 (5) (2016) 458–466, https://doi.org/10.1002/geot.201600033.
[24] A. Insana, M. Barla, Experimental and numerical investigations on the energy performance of a thermo-active tunnel, Renew. Energy 152 (2020) 781–792, https://doi.org/10.1016/j.renene.2020.01.086.
[25] F. Ronchi, D. Salciarini, N. Cavalagli, C. Tamagnini, Thermal response prediction of a prototype Energy Micro-Pile, Geomechanics for Energy and the Environment 16 (2018) 64–82, https://doi.org/10.1016/j.gete.2018.07.001.
[26] F. Cecinato, D. Salciarini, Energy performance assessment of thermo-active micro-piles via numerical modeling and statistical analysis, Geomechanics for Energy and the Environment 29 (2022), https://doi.org/10.1016/j.gete.2021.100268.

[27] M. Gerola, A. Lupattelli, F. Cecinato, D. Salciarini, T. Arola, Numerical Analysis of the Behaviour of Energy Micropiles Used for Heat Storage: a Case Study in Turku (Finland), Springer Series in Geomechanics and Geoengineering, 2023, pp. 808–815, https://doi.org/10.1007/978-3-031-34761-0_97.
[28] T.R. Andersen, S.E. Poulsen, K.W. Tordrup, The climate road – a multifunctional full-scale demonstration road that prevents flooding and produces green energy, Water (Switzerland) 14 (4) (2022) 666, https://doi.org/10.3390/w14040666.
[29] S.E. Poulsen, T.R. Andersen, K.W. Tordrup, Full-scale demonstration of combined ground source heating and sustainable urban drainage in roadbeds, Energies 15 (12) (2022) 4505, https://doi.org/10.3390/en15124505.
[30] R. Moffat, P. Reszka, M. Toledo, Use of retaining wall anchors as geothermal heat exchangers, Obras y Proyectos 32 (2022) 6–17, https://doi.org/10.21703/0718-51620202203201.
[31] T. Mimouni, F. Dupray, L. Laloui, Estimating the geothermal potential of heat-exchanger anchors on a cut-and-cover tunnel, Geothermics 51 (2014) 380–387, https://doi.org/10.1016/j.geothermics.2014.02.007.
[32] T. Mimouni, F. Dupray, S. Minon, L. Laloui, Heat Exchanger Anchors for thermo-active Tunnels. Swiss Association of Road and Transportation Experts, 2013.
[33] D. Adam, R. Markiewicz, Energy from earth-coupled structures, foundations, tunnels and sewers, Géotechnique 59 (3) (2009) 229–236, https://doi.org/10.1680/geot.2009.59.3.229.
[34] M. Gerola, V. Leclercq, P.J. Vardon, F. Cecinato, Energy Performance of Cutter Soil Mix Energy Walls: a Numerical Modelling Study, 2024. Manuscript Submitted.
[35] T. Du, Y. Li, X. Bao, W. Tang, H. Cui, Thermo-mechanical performance of a phase change energy pile in saturated sand, Symmetry 12 (11) (2020) 1781, https://doi.org/10.3390/sym12111781.
[36] A.F. Rotta Loria, E. Ravera, L. Laloui, Thermo-hydro-mechanical behavior of energy barrettes: field experiments and numerical simulations, Geomechanics for Energy and the Environment 34 (2023) 100451, https://doi.org/10.1016/j.gete.2023.100451.
[37] M. Ziegler, D. Koppmann, R. Pechnig, D. Knapp, Energy sheet pile walls – experimental and numerical investigation of innovative energy geostructures, XVII European Conference on Soil Mechanics and Geotechnical Engineering (2019).
[38] J. Haasnoot, P.J. Vardon, I. Pantev, S. Bersan, B. Bloemers, D. Smeulders, Energy quay walls, E3S Web of Conferences 205 (2020), https://doi.org/10.1051/e3sconf/202020506002.
[39] M. Gerola, F. Cecinato, V. Leclercq, P.J. Vardon, Energy quay walls: performance analysis and optimisation, Geomechanics for Energy and the Environment 42 (2025) 100664, https://doi.org/10.1016/j.gete.2025.100664.
[40] J. Zannin, A. Ferrari, M. Pousse, L. Laloui, Hydrothermal interactions in energy walls, Undergr. Space 6 (2) (2021) 173–184, https://doi.org/10.1016/j.undsp.2020.02.001.
[41] L. Laloui, M. Sutman, Energy geostructures: a new era for geotechnical engineering practice, in: Proc. XVII European Conference on Soil Mechanics and Geotechnical Engineering, 2019, pp. 1–15.
[42] A. Di Donna, F. Loveridge, M. Piemontese, M. Barla, The role of ground conditions on the heat exchange potential of energy walls, Geomechanics for Energy and the Environment 25 (2021) 100199, https://doi.org/10.1016/j.gete.2020.100199.
[43] M. Adinolfi, A.F. Rotta Loria, L. Laloui, S. Aversa, Experimental and numerical investigation of the thermo-mechanical behaviour of an energy sheet pile wall, Geomechanics for Energy and the Environment 25 (2021) 100208, https://doi.org/10.1016/j.gete.2020.100208.
[44] City of Amsterdam, Brief to the board of the city of Amsterdam regarding bridges and quay walls. https://www.k16.nl/werkgroep/Brief_kademuren.pdf, 2019.
[45] B. Sanner, Shallow geothermal energy-history, development, current status, and future prospects, in: European Geothermal Congress, 2016.
[46] J.P. De Vries, Quays Rather than Boilers, Extracting Heat from Water and Soil Through Energy Sheet Piles. Master Thesis, Delft University of Technology, 2021.